JURNAL LOCUS: Penelitian & Pengabdian
Volume 5 No. 8 August 2026
E-ISSN 2829-7334| P-ISSN 2829-5439
Hompage: https://locus.rivierapublishing.id/index.php/jl

Failure Analysis of First-Stage Vane in a GT13E1 Gas Turbine at Combined Cycle Power Plant

Mochammad Nafi Khumasi, Fahmi Mubarok*
Institut Teknologi Sepuluh Nopember, Indonesia
Email: 6007241020@its.ac.id, mubarok@its.ac.id*

Keywords:
Failure Analysis; Gas Turbine; First Stage Vane; Overheating; Scanning Electron Microscopy

Abstract

The first-stage vane of a GT13E1 gas turbine plays a critical role in directing high-temperature combustion gases toward the rotor blades and therefore operates under severe thermal conditions. During a field inspection at a combined-cycle power plant, significant damage was identified in the vane platform endwall region, including coating degradation, oxidation, and material loss, which resulted in hole formation. The damage was concentrated at the platform endwall corner. This study investigated the damage characteristics and failure mechanism through visual inspection, hardness testing, X-ray fluorescence (XRF) analysis, scanning electron microscopy (SEM), and metallographic examination. The results indicated localized overheating at the platform endwall corner. The silo comb geometry likely promoted secondary flow development and local turbulence, resulting in a non-uniform temperature distribution and the formation of hot spots near the endwall region. Elevated temperatures accelerated thermally grown oxide (TGO) layer formation at the coating interface, leading to thermal barrier coating (TBC) spallation. Subsequent exposure of the nickel-based alloy substrate promoted oxidation, erosion, microstructural degradation, and thermal fatigue crack initiation. Progressive crack propagation eventually caused structural damage to the vane platform. The findings indicate that localized thermal distress associated with secondary flow effects was the dominant failure mechanism and provide insights for inspection planning, cooling system design evaluation, and life management strategies for industrial gas turbine vanes.

INTRODUCTION

Gas turbines play a critical role in modern power generation systems due to their high efficiency and operational flexibility. In combined-cycle power plants (Brooks, 2000; Döbbeling et al., 2008), the reliability and availability of gas turbines are strongly influenced by the structural integrity of hot gas path components. Among these components, the first-stage vane is exposed to the most severe operating conditions because it directly encounters high-temperature combustion gases while regulating the flow direction toward the rotating blades (Brooks, 2000; Döbbeling et al., 2008).

The investigated component was a first-stage vane from a GT13E1 gas turbine operating at PLTGU Tanjung Priok. The vane was manufactured from an Inconel 939 nickel-based superalloy (Darolia, 2013; Bogdan & Peter, 2024) and protected by a thermal barrier coating (TBC) system. To reduce excessive metal temperatures, TBC systems are applied to protect the metallic substrate from extreme thermal exposure and extend component service life (Campbell et al., 2008; Chang et al., 2023). During routine inspection, severe degradation was identified at the platform endwall corner, characterized by coating spallation, oxidation, material loss, and crack formation.

The GT13E1 gas turbine employs a single-silo combustor configuration, in which hot combustion gases are discharged through a transition duct before entering the turbine section. Previous studies have reported that such flow configurations may generate complex inlet flow patterns and secondary-flow interactions near vane endwall regions, potentially resulting in localized thermal loading and accelerated degradation of hot gas path components (Wang et al., 2025; Gao et al., 2015; Shaikh, 2018). Previous investigations of gas turbine vane failures have predominantly focused on damage occurring at the leading-edge region, where components are directly exposed to high-temperature gas flow and severe thermal gradients. Although failure mechanisms such as thermal fatigue, oxidation, and cracking have been extensively studied in these areas, relatively limited attention has been given to degradation associated with thermal barrier coating (TBC) failure and thermally grown oxide (TGO) layer thickening. Therefore, this study focused on the degradation of the TBC system and the evolution of the TGO layer at the platform endwall corner region as the primary factors contributing to vane deterioration and failure.

Figure 1. (a) General view of first-stage vane consist of damage in platform endwall corner, (b) Macrography examination of damage

Source: Field Inspection Documentation, PLTGU Tanjung Priok (2024)

Damage to gas turbine hot gas path components has been extensively studied, with previous research identifying various failure mechanisms, including thermal fatigue, oxidation, hot corrosion, creep, and coating degradation (Ozaner et al., 2022; Raytpour & Mehdizadeh, 2025; Ruggieri, 2024). Studies have shown that the leading-edge region is particularly susceptible to thermal fatigue cracking due to high thermal gradients and cyclic loading, whereas the platform endwall region has received comparatively less attention despite its complex flow dynamics and potential for localized overheating. Fathyunes and Mohtadi-Bonab (2023) reviewed corrosion and fatigue failure mechanisms in gas turbines, highlighting the importance of understanding degradation progression in critical components. Barwinska et al. (2023) synthesized research on thermal barrier coatings (TBCs) for nickel-based superalloys, emphasizing the role of thermally grown oxide (TGO) layer formation and growth in coating spallation. Scotson et al. (2024) reviewed characterization techniques for investigating TBC and environmental barrier coating (EBC) failures, while Anusha et al. (2025) examined advancements in high-velocity oxygen fuel (HVOF)-sprayed coatings for high-temperature durability. However, limited studies have specifically addressed the failure mechanisms associated with platform endwall corner degradation, where secondary flow interactions and localized hot spot formation may accelerate coating deterioration and substrate damage. Zhou et al. (2023) demonstrated the application of micro-beam X-ray fluorescence spectroscopy for quantitative characterization of elemental segregation in superalloys, while Miller (2009) provided a historical perspective on TBC development for gas turbine engines. Rai et al. (2009) investigated calcium–magnesium–alumino–silicate (CMAS)-resistant TBCs, and Anderson (2005) established fundamental principles of fracture mechanics applicable to crack propagation analysis. Lee et al. (2021) reviewed surface finishing processes for metal additive-manufactured components, and Shaikh et al. (2023) examined the as-built microstructure of additively manufactured Inconel 939. Murphy et al. (2001) analyzed the as-deposited mixed zone in the TGO layer beneath TBCs, while Mehboob et al. (2020) reviewed failure mechanisms and strategies for extending TBC lifetime. Raza et al. (2024) systematically reviewed the development of Inconel 939 alloys through additive manufacturing. Despite these contributions, the specific failure mechanism occurring at the platform endwall corner region, where TBC degradation, TGO thickening, and localized overheating interact synergistically, remains insufficiently understood.

The novelty of this research lies in its focused investigation of platform endwall corner failure in a GT13E1 first-stage vane by combining multiple characterization techniques to elucidate the degradation sequence, from TBC spallation and substrate oxidation to microstructural degradation and crack propagation, with particular emphasis on the role of TGO evolution. This research also provides empirical evidence regarding the thermal degradation gradient and hardness reduction profile associated with localized overheating in the endwall region, offering insights for inspection planning, cooling design evaluation, and life management of industrial gas turbine vanes. The findings are expected to benefit power plant operators by enabling the identification of early signs of endwall degradation during routine inspections, assist maintenance engineers in prioritizing inspection areas and scheduling interventions, support gas turbine manufacturers in evaluating cooling design effectiveness and developing improved cooling configurations, and provide a reference for researchers investigating TBC degradation mechanisms and failure analysis of superalloy components. This study aimed to investigate the damage characteristics and failure mechanism through visual inspection, hardness testing, X-ray fluorescence (XRF) analysis, scanning electron microscopy (SEM), and metallographic examination, with the objective of identifying the root cause of vane failure and providing recommendations to prevent similar degradation during future service.

METHOD

The failure analysis was conducted using an integrated experimental approach that combined compositional analysis, mechanical testing, microstructural characterization, and phase identification to investigate the degradation mechanism of the vane platform endwall. Initial evaluation was performed through macroscopic observation to identify damage morphology, coating condition, oxidation features, and crack distribution, which also provided the basis for selecting critical sampling locations (Ozaner et al., 2022).

The chemical composition of the material was then examined using X-ray fluorescence (XRF) analysis to verify the base alloy and assess its conformity with Inconel 939 specifications. Microstructural characterization was performed through metallographic examination to evaluate grain structure, gamma prime (γ') morphology, carbide distribution, and potential microstructural degradation associated with high-temperature exposure. Changes in mechanical properties were evaluated using micro-Vickers hardness testing to assess the effect of thermal loading on material strength across different regions (Raytpour & Mehdizadeh, 2025).

Further analysis of surface degradation and crack characteristics was conducted using scanning electron microscopy (SEM) to observe crack initiation sites, oxidation layers, and coating–substrate interactions. Energy-dispersive spectroscopy (EDS) was employed to evaluate elemental distributions and identify oxidation products, particularly those associated with thermally grown oxide (TGO) formation. Phase identification was performed to detect the base alloy phases and oxide phases formed during service exposure (Ruggieri, 2024).

The experimental results were interpreted based on the high-temperature behavior of nickel-based superalloys, degradation mechanisms of thermal barrier coating (TBC) systems, and heat transfer characteristics in gas turbine environments. Particular attention was given to localized overheating at the platform endwall, which may have resulted from secondary flow interactions and reduced cooling effectiveness. Through this integrated approach, the relationship between thermal exposure, coating degradation, oxidation, and crack propagation was systematically evaluated to determine the root cause of the vane failure (Fathyunes & Mohtadi-Bonab, 2023).

RESULTS AND DISCUSSION

Visual Inspection and Damage Morphology

The macroscopic examination of the first-stage vane revealed that the most severe damage was localized at the platform endwall corner region. Figure 1(b) shown the affected area exhibited coating degradation, dark surface discoloration, oxidation products, material loss, and visible crack formation. In contrast, the airfoil surface and cooling hole rows remained relatively intact, indicating that the damage was not initiated from conventional cooling-hole-related stress concentration.

The morphology of the damaged region suggests localized thermal distress characterized by excessive temperature exposure. The presence of severe oxidation and geometric distortion indicates that the protective TBC system had deteriorated prior to significant substrate damage. Once the coating was lost, the Inconel 939 substrate was directly exposed to high-temperature combustion gases, leading to progressive oxidation and weakening of the material.

These observations support the hypothesis that the failure originated from localised overheating at the platform endwall, likely due to secondary flow interactions and reduced cooling effectiveness in this region.

Chemical Composition Analysis

The chemical composition analysis was performed using X-ray fluorescence (XRF) to verify the material of the vane and evaluate its conformity with the nominal composition of Inconel 939. The measured composition is presented in Table 1 and compared with the standard composition range of Inconel 939 (Bogdan & Peter, 2024). The results show that the major alloying elements, including chromium (Cr), cobalt (Co), and titanium (Ti), are within or close to the expected range of Inconel 939. Although several elements such as aluminum (Al), tantalum (Ta), and tungsten (W) were not detected in the analysis, the overall composition remains consistent with a nickel-based superalloy system. The measured nickel (Ni) content is approximately 51.2 wt.%, indicating that Ni remains the dominant element in the alloy. However, it should be noted that the absence of several minor elements in the measurement may affect the calculated balance of Ni.

Overall, the chemical composition confirms that the investigated vane material corresponds to IN939, and therefore, the observed failure is not attributed to material composition deficiency but is more likely related to service-induced degradation such as localized overheating and coating failure (Barwinska et al., 2023).

Table 1. Composition of Inconel 939

Element	Cr	Co	Ti	Al	C	Nb	Ta	W	Ni
Standart (wt%)*	22	19	4	2	0.2	1	1.4	1.9	Balance
Measured (wt%)	21.3	20.0	3.47	ND	ND	1.5	ND	ND	51.2

*EOS Gmbh (2025)

Hardness Analysis

Microhardness measurements were performed along a line extending from the exposed failure surface toward the underlying base material to evaluate the influence of thermal exposure on the mechanical properties of the Inconel 939 substrate. The locations of the hardness indentations are shown in Figure. 2 (a), while corresponding hardness profile is presented in figure 2 (b).

The hardness profile exhibits a pronounced gradient from the exposed failure surface toward the interior of the vane. The lowest hardness value of 155 HVN was recorded at a distance of 0.07 mm from the exposed surface. Within approximately 0.72 mm from the surface, hardness values remained relatively low, ranging between 155 and 227 HVN. This region is identified as a thermally degraded zone, where prolonged exposure to elevated temperatures following the loss of thermal protection promoted microstructural degradation and material softening (Scotson et al., 2024).

Beyond approximately 0.72 mm from the exposed surface, hardness values increased significantly and generally ranged between 250 and 350 HVN. Although several localized measurements exceeded 330 HVN, the overall hardness distribution remained relatively stable within the range commonly reported for service-exposed Inconel 939. The observed fluctuations are attributed to normal microstructural variations within the cast superalloy, including differences in precipitate distribution, carbide morphology, and local dendritic segregation.

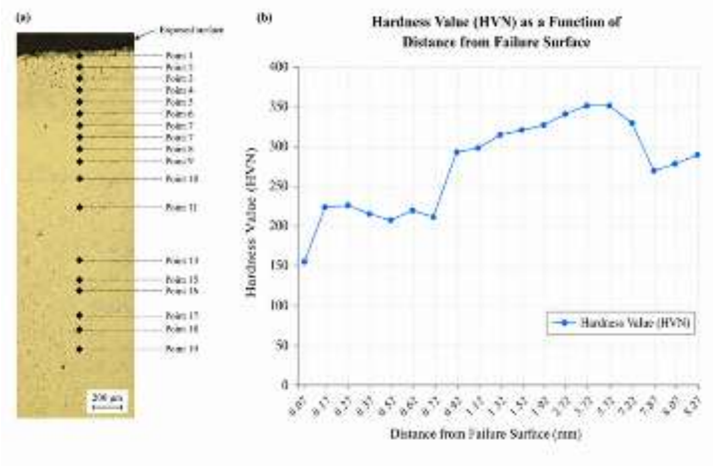

Figure 2. Microhardness evaluation in damage cross-section : (a) Indentitation location, (b) Hardness profile

Source: Author's Laboratory Analysis (2024)

At greater distances from the failure surface, the hardness profile became relatively stable, generally ranging between 250 and 320 HVN. This region is interpreted as the underlying Inconel 939 base material, where the original strengthening mechanisms remained largely preserved. The relatively constant hardness values indicate that thermal degradation was predominantly localized near the exposed surface and did not penetrate deeply into the substrate.

Although several measurement points exhibited hardness values exceeding 330 HVN, the overall trend demonstrates that the base material maintained hardness within the expected range for service-exposed Inconel 939. The gradual transition from severely softened surface material to stable substrate hardness confirms the existence of a thermal degradation gradient extending inward from the failure surface (Anusha et al., 2025).

The overall hardness distribution demonstrates that thermal degradation was highly localized near the exposed surface and progressively decreased with increasing distance from the damaged region. This observation is consistent with the metallographic evidence, which revealed a corresponding transition from a severely degraded microstructure near the surface to a comparatively less affected substrate (Zhou et al., 2023).

Metalographic Analysis

Metallographic examination was conducted to evaluate the microstructural condition of the investigated vane material and to identify degradation associated with service exposure. The material is identified as Inconel 939, a nickel-based superalloy characterized by a γ matrix strengthened by γ’ precipitates. Representative microstructures of the reference and damaged regions are presented in Figure 3. The reference microstructure Figure. 3 (a) shows a typical equiaxed grain structure with clearly defined grain boundaries. Carbide particles are observed along the grain boundaries, which are commonly associated with $M_{23}C_6$ carbides in nickel-based superalloys and contribute to grain boundary strengthening. At higher magnification Figure. 3 (b), fine and uniformly distributed γ’ precipitates are observed within the γ matrix. The homogeneous distribution and small size of the γ’ phase indicate that the material is in a stable condition without significant thermal degradation. In contrast, the damaged region exhibits a clear microstructural gradient from the surface toward the interior, as shown in Figure. 3 (c). The near-surface region appears significantly degraded, characterized by a darkened layer and the absence of a clearly defined γ/γ’ structure. This condition indicates severe oxidation and material degradation, suggesting that the protective coating system had deteriorated, exposing the substrate directly to high-temperature combustion gases. Beneath this degraded surface, the microstructure gradually transitions toward a more recognizable γ/γ’ morphology (Miller, 2009).

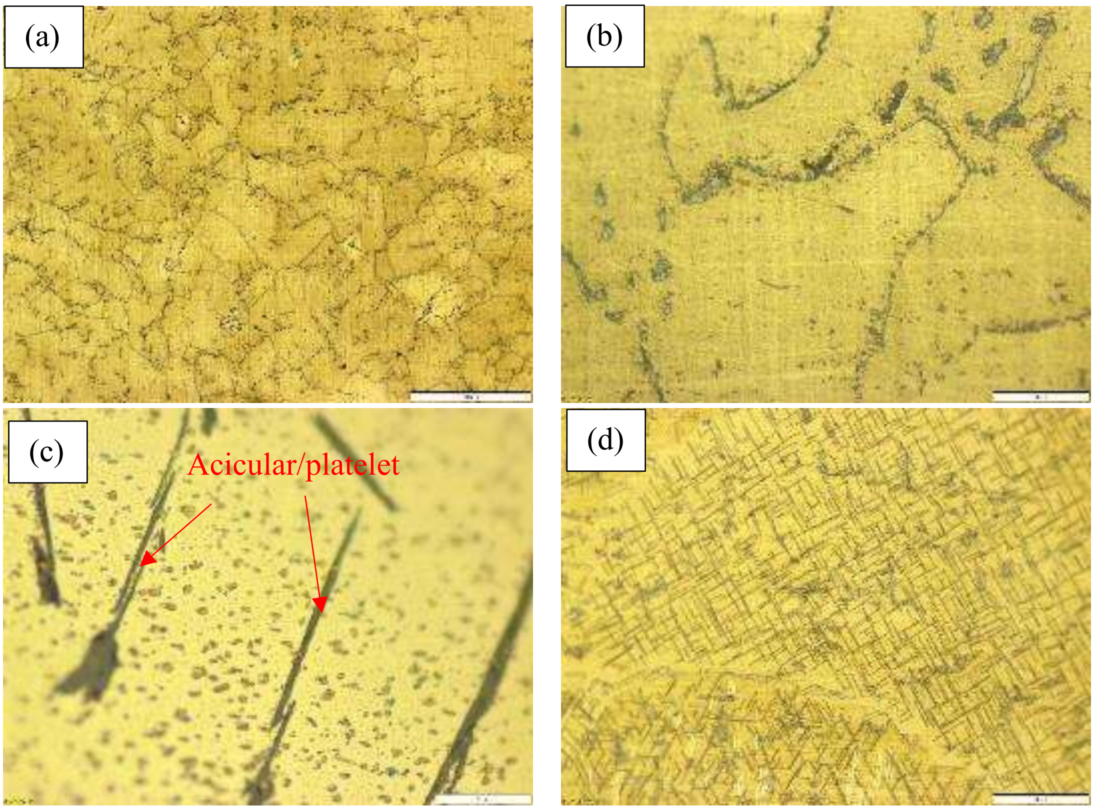

Figure 2. Metallographic microstructure of first stage vane: (a-b) reference region, (c) damaged region , (d) base metal region.

Source: Author's Laboratory Analysis (2024)

Further microstructural changes are observed in the damaged region near the crack area, as shown in Figure. 3 (d). The microstructure exhibits a less homogeneous morphology compared with the reference region, suggesting microstructural evolution associated with prolonged thermal exposure. In addition, elongated acicular or platelet-like features were observed in the degraded region. The formation of these morphologies is commonly associated with microstructural instability during prolonged thermal exposure in nickel-based superalloys. However, definitive phase identification was beyond the scope of the present investigation (Rai et al., 2009).

Overall, the metallographic observations indicate that degradation initiated at the exposed surface and progressively decreased toward the interior of the vane. The observed microstructural gradient, together with the hardness profile and oxidation evidence, supports the hypothesis that localized thermal exposure played a dominant role in the degradation process. These findings are consistent with the proposed failure mechanism in which localized hot-spot formation accelerated coating degradation, substrate overheating, and subsequent microstructural deterioration (Anderson, 2005).

SEM-EDS Analysis

To further investigate the degradation mechanism of the first-stage vane, Scanning Electron Microscopy coupled with Energy Dispersive Spectroscopy (SEM-EDS) was performed on representative regions of the damage cross-section crack cross-section, and degraded surface. SEM observation revealed the presence of an acicular or needle-like microstructure embedded within the matrix, as shown in Figure 4 (b). This morphology was not observed in the reference specimen and is therefore considered a product of microstructural evolution during service exposure. EDS analysis performed on the acicular feature indicated significant aluminum enrichment, with the aluminum content reaching approximately 61 wt%, whereas the surrounding matrix retained the characteristic composition of Inconel 939 dominated by Ni, Cr, and Co. The formation of the acicular structure suggests that prolonged thermal exposure promoted phase transformation and microstructural instability within the substrate material (Lee et al., 2021).

The next examination was conducted on the crack cross-section, as presented in Figure 5 (a). SEM images revealed oxidation products distributed along the crack path and adjacent grain boundaries shown in Figure 5 (b). EDS measurements detected elevated oxygen concentrations within these regions, indicating that high-temperature oxidation propagated inward through preferential diffusion paths. The presence of oxygen-rich phases inside the crack suggests that oxidation was not limited to the external surface but continued to develop progressively into the material after crack initiation (Shaikh et al., 2023).

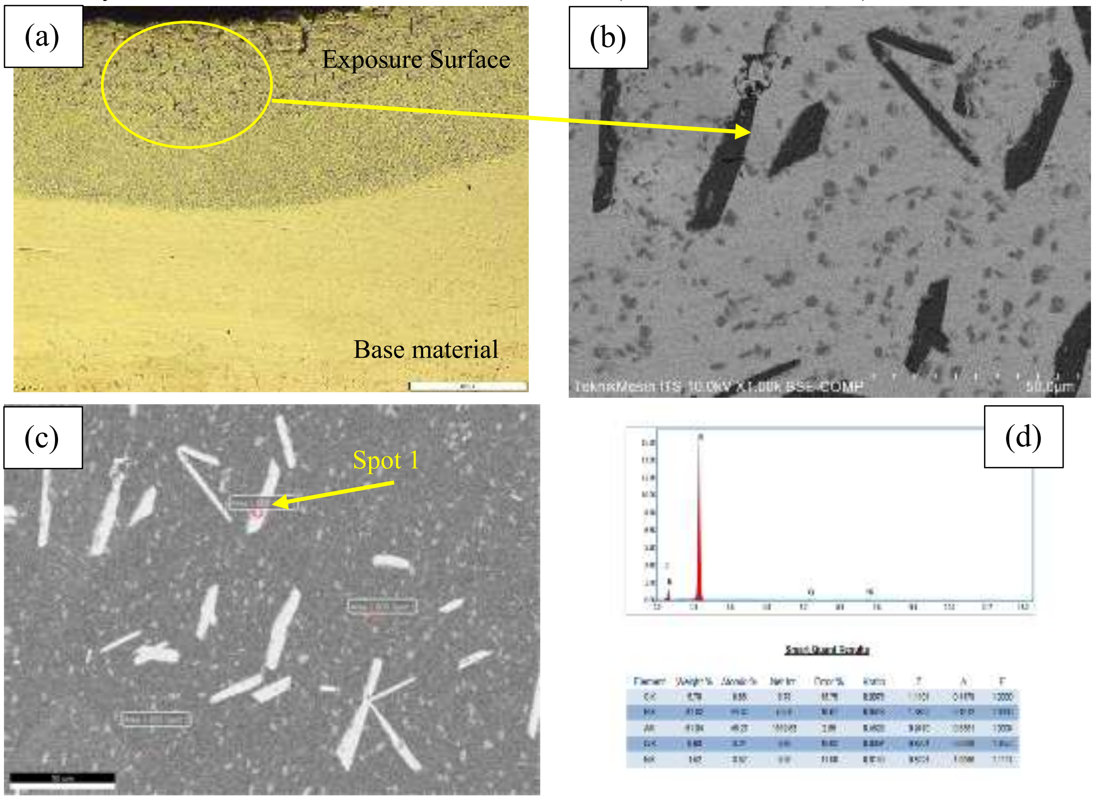

Figure 3. Identification of damage cross-section in failed vane : (a) Investigation region, (b) SEM image of precipitates, (c) EDS analysis location, (d) EDS spectrum result.

Source: Author's Laboratory Analysis (2024)

The morphology of the degraded surface is shown in Figure 6 (a). The exposed surface exhibited a rough and heterogeneous appearance characterized by microcracks, porosity, granular features, and oxidation products. Several regions displayed in Figure 6 (b) significant contrast differences, indicating variations in composition and degradation severity. EDS analysis in Figure 6 (d) confirmed the presence of oxygen-rich areas, demonstrating that extensive oxidation occurred after the thermal barrier coating system lost its protective function and the substrate became directly exposed to hot combustion gases.

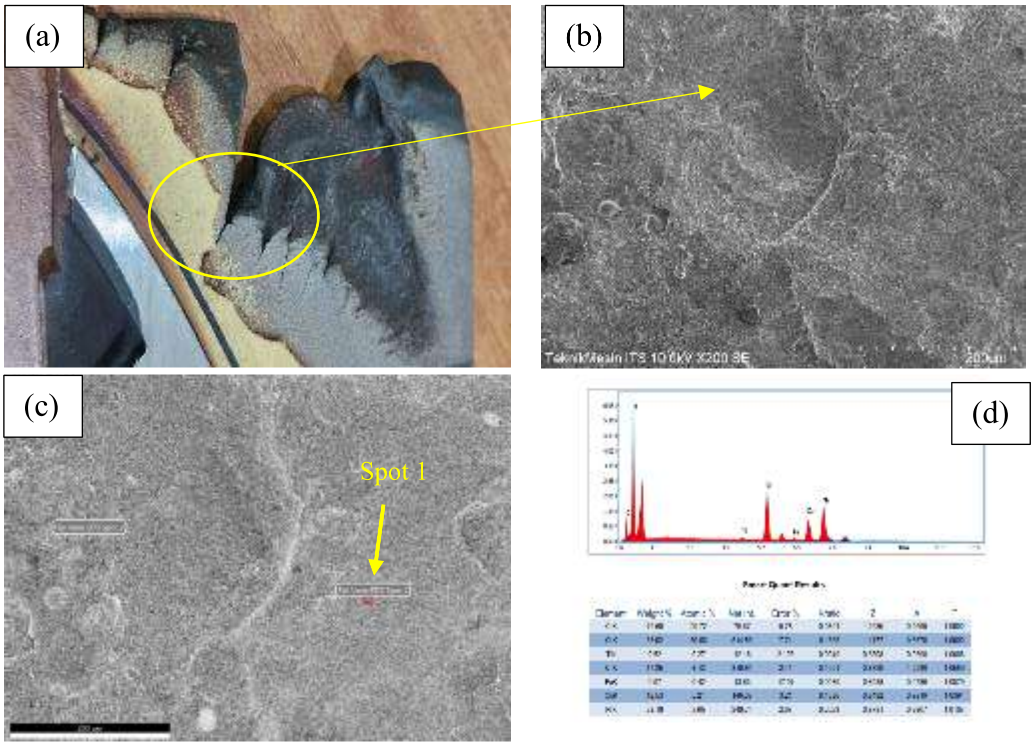

Figure 5. Idenfication of crack cross-section in failed vane : (a) Investigation region, (b) SEM image, (c) EDS analysis spot location. (d) EDS spectrum result.

Source: Author's Laboratory Analysis (2024)

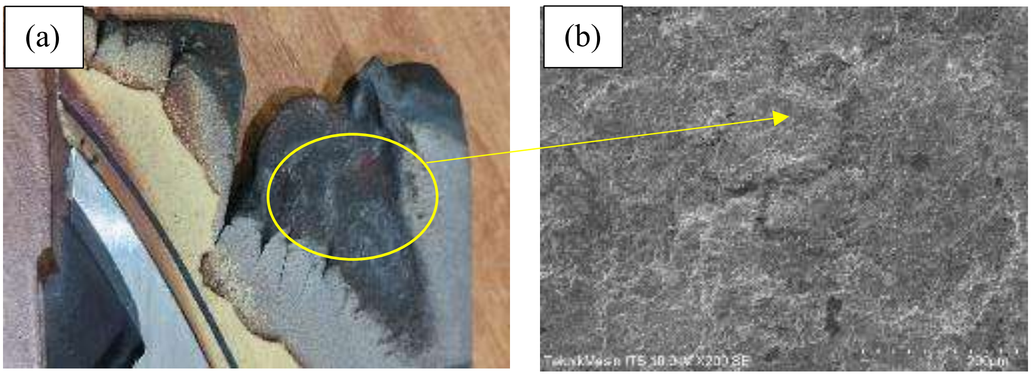

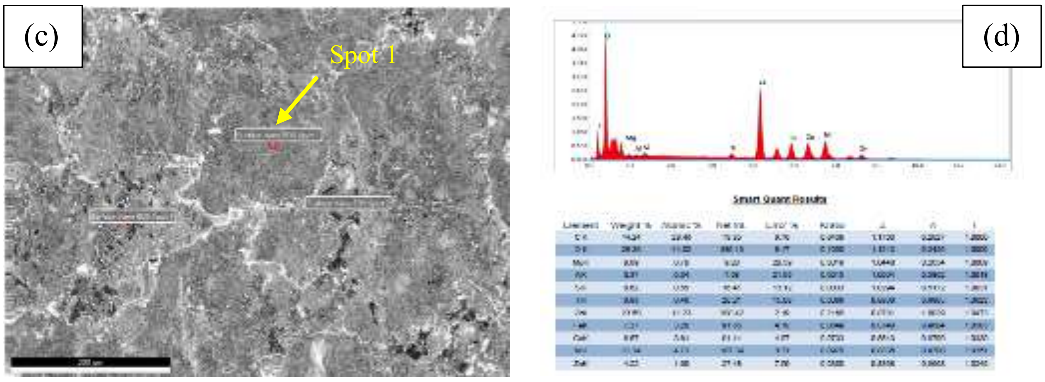

Figure 6. Idenfication of damage surface in failed vane : (a) Investigation region, (b) SEM image, (c) EDS analysis spot location. (d) EDS spectrum result.

Source: Author's Laboratory Analysis (2024)

The SEM-EDS observations are consistent with the hardness and metallographic results discussed previously. The occurrence of acicular structures, oxygen enrichment, oxidation along crack paths, and severe surface degradation confirms that the vane experienced substantial thermal damage during service. These findings indicate that deterioration of the thermal barrier coating system promoted oxidation and microstructural degradation of the Inconel 939 substrate, ultimately contributing to crack propagation and progressive material loss (Murphy et al., 2001).

Failure Mechanism

Based on the results obtained from visual inspection, hardness testing, metallographic examination, and SEM-EDS characterization, a failure mechanism is proposed to explain the degradation of the first-stage vane. The proposed degradation sequence, developed from the experimental observations and supported by established degradation mechanisms reported in the literature, is summarized in Figure 7.

The degradation process is believed to have initiated during long-term operation under repeated thermal cycling conditions, as illustrated in stages 1–3 of Figure 7. Continuous exposure to high-temperature combustion gases from single-silo combustor configuration promoted progressive deterioration of the coating system. Oxidation occurring at the coating interface likely contributed to degradation of the protective layers and accumulation of thermal stresses resulting from thermal expansion mismatch between the coating system and the substrate. Although the formation and growth of a thermally grown oxide (TGO) layer were not directly examined in the present study, such mechanisms have been widely reported as contributing factors in TBC degradation (Mehboob et al., 2020).

The loss of the protective TBC exposed the underlying Inconel 939 substrate directly to the hot combustion gas environment. As a result, the local metal temperature increased, accelerating oxidation and microstructural degradation of the exposed material as illustrated in stage 4 of Figure 7. This condition significantly reduced the effectiveness of the thermal protection system and increased the local metal temperature (Raza et al., 2024).

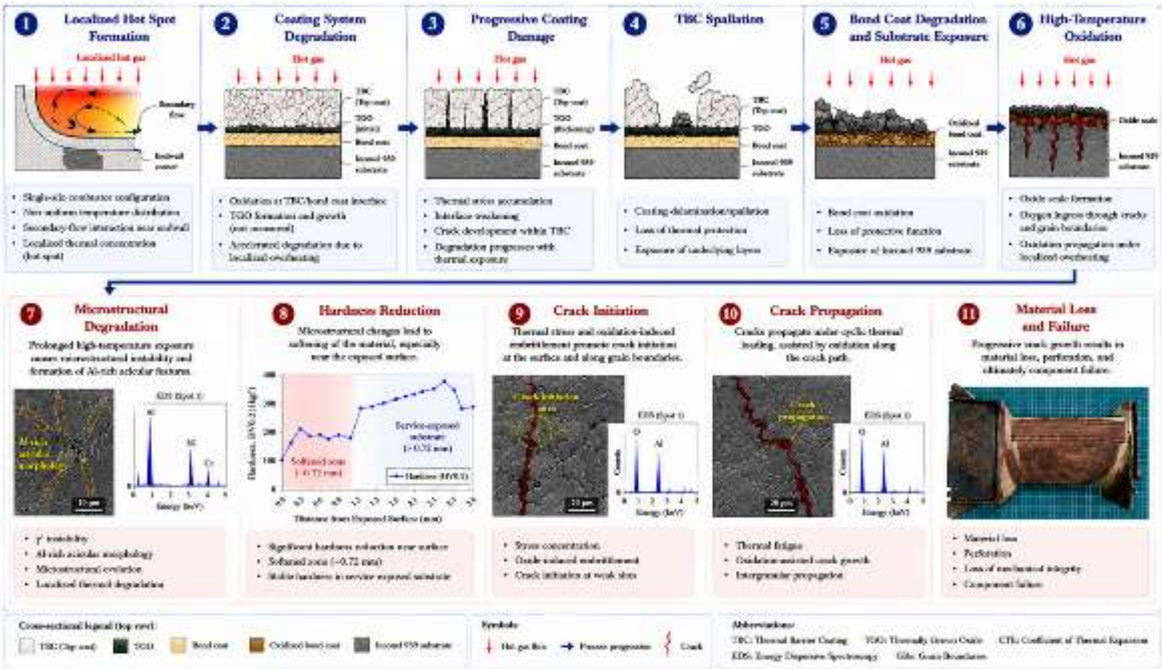

Figure 7. Proposed Failure Mechanism of GT 13E1 First-stage Vane Based On Experimental Observations

Source: Author's Analysis and Synthesis (2024)

Following exposure of the substrate, high-temperature oxidation progressively developed at the surface and propagated through grain boundaries and existing defects. This mechanism was supported by SEM-EDS analysis, which revealed elevated oxygen concentrations within the degraded region and along crack paths as shown in stage 5-6 of Figure 7. The presence of oxygen-rich areas indicates the formation of oxide products during service exposure. In addition, the observation of oxidized cracks suggests that oxidation occurred before or during crack propagation, contributing to the deterioration of material integrity and facilitating crack initiation.

Simultaneously, prolonged thermal exposure caused significant microstructural changes within the Inconel 939 substrate. As presented in stage 7 of Figure 7, metallographic observations revealed precipitate coarsening, acicular phase formation, and indications of carbide evolution compared with the expected microstructure of the alloy. These microstructural changes indicate thermal degradation of the strengthening phases and reduced resistance to high-temperature service conditions.

The reduction in mechanical properties was further evidenced by the hardness measurements. The hardness profile showed severe softening near the exposed surface as hardness profile shown in stage 8 of Figure 7. This hardness gradient demonstrates that hardness values were substantially lower than those measured in the underlying base material, indicating localized softening caused by thermal degradation and oxidation.

The combined effects of oxidation, microstructural degradation, localized hot-spot formation, and mechanical softening eventually facilitated crack initiation and propagation under cyclic thermal loading conditions as illustrated in stage 9-10 of Figure 7. As crack growth continued during operation, progressive material loss occurred within the platform endwall region, ultimately producing the severe damage morphology observed during inspection.

Ultimately, the failure of the investigated first-stage vane is attributed to a synergistic degradation mechanism involving coating spallation, localized overheating, flow-induced hot-spot formation caused by surface irregularities, high-temperature oxidation, microstructural deterioration of Inconel 939, reduction in hardness, and progressive crack propagation under thermal cyclic loading conditions. Since direct evidence of TGO thickness evolution was not obtained in this investigation, excessive TGO growth is considered a plausible contributing factor to coating degradation based on established TBC degradation mechanisms, but it cannot be conclusively verified from the present experimental results mechanisms, but it cannot be conclusively verified from the present experimental results.

CONCLUSIONS

Visual inspection revealed extensive coating loss, cracking, and significant material loss in the platform endwall corner region. These observations indicated that degradation of the thermal protection system had occurred prior to the observed substrate damage. Chemical composition analysis confirmed that the investigated component was manufactured from Inconel 939 and complied with the nominal composition requirements of the alloy. Therefore, the failure was not associated with material selection or compositional deficiencies. Hardness measurements revealed a pronounced hardness gradient from the exposed failure surface toward the unaffected base material. A degraded surface layer extending approximately 0.72 mm from the failure surface exhibited significant softening, with the lowest hardness value reaching 155 HVN, while the underlying substrate maintained considerably higher hardness values. Metallographic and SEM-EDS examinations identified evidence of thermal degradation, including acicular phase formation, precipitate coarsening, carbide evolution, oxidation products, and oxygen enrichment along degraded regions and crack paths. These observations indicated substantial microstructural deterioration caused by prolonged exposure to elevated temperatures. The failure of the GT13E1 first-stage vane was primarily attributed to progressive thermal barrier coating (TBC) system degradation, followed by loss of thermal protection, high-temperature oxidation, microstructural degradation of the Inconel 939 substrate, localized hardness reduction, and oxidation-assisted crack propagation under cyclic thermal operating conditions. These processes ultimately resulted in severe material loss and component failure.

REFERENCES

Anderson, T. L. (2005). *Fracture mechanics: Fundamentals and applications*. CRC Press. https://doi.org/10.1201/9781420058215

Anusha, K., Chakrabarty, S., Routara, B., Kumar, N., & Guha, S. (2025). A review on advancements in HVOF sprayed coating of MCrAlX: Innovations in processing, performance, applications, and high-temperature durability. *Discover Materials, 5*(2). https://doi.org/10.1007/s43939-025-00416-2

Barwinska, I., Kopec, M., Kukla, D., Senderowski, C., & Kowalewski, Z. L. (2023). Thermal barrier coatings for high-temperature performance of nickel-based superalloys: A synthetic review. *Coatings, 13*(4), 1–21. https://doi.org/10.3390/coatings13040769

Bogdan, M., & Peter, I. (2024). A comprehensive understanding of thermal barrier coatings (TBCs): Applications, materials, coating design and failure mechanisms. *Metals, 14*(5), 575–608. https://doi.org/10.3390/met14050575

Brooks, F. J. (2000). *GE gas turbine performance characteristics*. GE Power Systems.
Campbell, A., Goldmeer, J., Healy, T., Washam, R., Molière, M., & Citeno, J. (2008). Heavy duty gas turbines fuel flexibility. https://doi.org/10.1115/GT2008-51368
Chang, S. W., Wu, P. S., Wan, T. Y., & Cai, W. L. (2023). A review of cooling studies on gas turbine rotor blades with rotation. *Inventions, 8*(1). https://doi.org/10.3390/inventions8010021
Darolia, R. (2013). Thermal barrier coatings technology: Critical review, progress update, remaining challenges and prospects. *International Materials Reviews, 58*(6), 315–348. https://doi.org/10.1179/1743280413Y.0000000019
Döbbeling, K., Meeuwissen, T., & Zajadatz, M. (2008). Fuel flexibility of the Alstom GT13E2 medium sized gas turbine. https://doi.org/10.1115/GT2008-50950
Fathyunes, L., & Mohtadi-Bonab, M. A. (2023). A review on the corrosion and fatigue failure of gas turbines. *Metals, 13*(4). https://doi.org/10.3390/met13040701
Gao, S., Wang, L., Feng, C., Xiao, Y., & Ketui, D. (2015). Monitoring temperature for gas turbine blade: Correction of reflection model. *Optical Engineering, 54*(6), 065102. https://doi.org/10.1117/1.OE.54.6.065102
Lee, J.-Y., Nagalingam, A. P., & Yeo, S. H. (2021). A review on the state-of-the-art of surface finishing processes and related ISO/ASTM standards for metal additive manufactured components. *Virtual and Physical Prototyping, 16*(1), 68–96.
Mehboob, G., Liu, M.-J., Xu, T., Hussain, S., Mehboob, G., & Tahir, A. (2020). A review on failure mechanism of thermal barrier coatings and strategies to extend their lifetime. *Ceramics International, 46*(7), 8497–8521. https://doi.org/10.1016/j.ceramint.2019.12.200
Miller, R. A. (2009). *History of thermal barrier coatings for gas turbine engines*. NASA Glenn Research Center.
Murphy, K. S., More, K. L., & Lance, M. J. (2001). As-deposited mixed zone in thermally grown oxide beneath a thermal barrier coating. *Surface and Coatings Technology, 146–147*, 152–161. https://doi.org/10.1016/S0257-8972(01)01371-8
Ozaner, O. C., Karabulut, Ş., & İzciler, M. (2022). Study of the surface integrity and mechanical properties of turbine blade fir trees manufactured in Inconel 939 using laser powder bed fusion. *Journal of Manufacturing Processes, 79*, 47–59. https://doi.org/10.1016/j.jmapro.2022.04.054
Rai, A., Bhattacharya, R., & Eden, T. (2009). CMAS-resistant thermal barrier coatings (TBC). *International Journal of Applied Ceramic Technology, 7*(5), 662–674. https://doi.org/10.1111/j.1744-7402.2009.02373.x
Raytpour, M., & Mehdizadeh, M. (2025). Failure analysis of the first stage vane of the gas turbine. *Engineering Failure Analysis, 170*, 109281. https://doi.org/10.1016/j.engfailanal.2025.109281
Raza, S., Canyurt, O., & Sezer, H. K. (2024). A systematic review of Inconel 939 alloy parts development via additive manufacturing process. *Heliyon, 10*(3), e25506. https://doi.org/10.1016/j.heliyon.2024.e25506
Ruggieri, A. (2024). *The influence of hot isostatic pressing performed above solidus temperature of LPBFed Inconel 939 for microstructural improvement* (Master's thesis). Politecnico di Torino.
Scotson, D., Paksoy, A. H., & Xiao, P. (2024). Characterisation techniques for investigating TBC and EBC failure: A review. *Frontiers in Ceramic Engineering, 1*, 1–27. https://doi.org/10.3389/fceic.2023.1307437
Shaikh, A. S. (2018). *Development of a γ′ precipitation hardening Ni-base superalloy for additive manufacturing* (Master's thesis). Chalmers University of Technology.
Shaikh, A. S., Rashidi, M., Minet-Lallemand, K., & Hryha, E. (2023). On as-built

microstructure and necessity of solution treatment in additively manufactured Inconel 939. *Powder Metallurgy, 66*(1), 3–11. https://doi.org/10.1080/00325899.2022.2041787

Wang, X., Cui, Y., Zhou, Y., Li, Z., Zhao, Y., & Wang, J. (2025). The microstructure evolution of a Ni-based superalloy turbine blade at elevated temperature. *Coatings, 15*(7), 1–11. https://doi.org/10.3390/coatings15070835

Zhou, X., et al. (2023). Quantitative characterization of elemental segregation in Inconel 718 superalloy by micro-beam X-ray fluorescence spectroscopy and its correlation study. *Materials, 16*(22), 7163. https://doi.org/10.3390/ma16227163